

Denoising of  $B_z$  data for conductivity  
reconstruction in magnetic resonance electrical  
impedance tomography (MREIT)

by

Chang-Ock Lee, Seonmin Ahn and Kiwan Jeon

BK21 Research Report

09 - 16

June 30, 2009

DEPARTMENT OF MATHEMATICAL SCIENCES

The second stage of  
**BK21**  
Fostering A World Class Talent

**KAIST**

**한국과학기술원**  
Korea Advanced Institute of Science and Technology

# Denoising of $B_z$ Data for Conductivity Reconstruction in Magnetic Resonance Electrical Impedance Tomography (MREIT)\*

Chang-Ock Lee<sup>†</sup>, Seonmin Ahn<sup>‡</sup>, and Kiwan Jeon<sup>§</sup>

Department of Mathematical Sciences, KAIST  
Daejeon, 305-701, Korea

## Abstract

This paper proposes effective partial differential equation(PDE)-based denoising techniques for magnetic resonance electrical impedance tomography (MREIT). MREIT is an imaging tool which provides cross-sectional conductivity images of a target object. If we inject currents to a target object, MREIT measures the induced magnetic flux density  $B_z$  and reconstructs conductivity images. Due to the fact that this tool utilizes the Laplacian of  $B_z$ , the data quality is significant in the reconstruction. However in *in vivo* experiments and medical applications to humans, the measured  $B_z$  has low SNR since we cannot use high magnitude currents. Furthermore, the  $B_z$  data has salt-pepper type noise in outer layers of bones and gas-filled organs. Hence the reconstructed conductivity will not be reliable without the effective denoising. We propose modifications of the Hahn-Lee method [1] for denoising  $B_z$ . The Hahn-Lee method is remarkable in its ability to remove noise from normal images, however, modifications are necessary for applications to  $B_z$  due to the data properties; the data is microscale and the ramp structure is very weak. The proposed modifications enable us to magnify the effects of ramp-strength and to perform isotropic smoothing in salt-pepper type noisy regions which are identified through eigenvalue analysis while we use anisotropic smoothing for preserving ramp structure in the other regions. We show that the modified Hahn-Lee method performs effectively in noise removal from  $B_z$  through evaluations using three different noisy data sets: a simulated phantom, an experimental phantom, and a post-mortem canine brain.

**Key words:** conductivity image, MREIT, PDE-based ramp preserving denoising.

## 1 Introduction

In recent years, numerous studies have attempted to develop algorithms which reconstruct cross sectional conductivity images from magnetic resonance electrical impedance tomography (MREIT). Among the developed algorithms, the harmonic  $B_z$  algorithm gives the most remarkable conductivity images from MREIT data in phantom, post-mortem and *in vivo* animal experiments as studied in [2, 3, 4, 5]. In addition, it is more practical than other algorithms. Generally, all three components of magnetic flux density

---

\*This work was supported by NRF grant funded by the Korea government (MEST)(R11-2002-103).

<sup>†</sup>colee@kaist.edu, corresponding author

<sup>‡</sup>minnim@kaist.ac.kr

<sup>§</sup>Jeonkiwan@kaist.ac.kr

$B = (B_x, B_y, B_z)$  are necessary to reconstruct conductivity images and it leads to repeat experiments three times with rotating a target object. In contrast, the harmonic  $B_z$  algorithm reconstructs conductivity images solely by the main magnetic directional component  $B_z$ . Thus it reduces the number of experiments by one third, and becomes applicable to human experiments in the view of the present MR-technology which does not provide rotations.

For medical MREIT applications to humans, it is necessary to use low magnitude currents due to safety regulations. However, manipulation with low magnitude currents brings about low SNR of  $B_z$ . Low SNR is problematic since the Laplacian of  $B_z$  is required in the reconstruction process. The noise effect is amplified significantly in differentiating  $B_z$ , and it deteriorates the quality of results. Hence the reconstructed conductivity will not be reliable without effective removal of noise.

To remove noise from  $B_z$ , Lee *et al.* [6] proposed the harmonic decomposition method. By the harmonic decomposition, the  $B_z$  data is divided into smooth harmonic and peak-structural parts. The main idea of this method is reforming the refracted  $B_z$  structure to peak-structure by extracting the harmonic part of  $B_z$  and denoising only the peak-structural part. In addition, this method utilizes the MR magnitude image which is obtained spontaneously in MREIT experiments. However, this method does not provide accurate Laplacian information of  $B_z$  since it is one of edge preserving denoising schemes based on the Perona-Malik method [7]. It is required to denoise  $B_z$  with ramp preserving denoising scheme for the accurate Laplacian information.

Gilboa *et al.* [8] suggested the complex diffusion method. It is a ramp preserving denoising method with a new scheme of representing the second derivative information of a target image using complex valued coefficient. However this method has no tools to handle salt-pepper type noise which is originated from animals and human body especially in outer layers of bones and gas-filled organs. In these parts, the magnitude of MR signal is extremely low, thus we are not able to obtain  $B_z$  robustly and it results in salt-pepper type noise.

Hahn and Lee [1] proposed another ramp preserving denoising method which utilizes a structure tensor. In this paper, we present a scheme of finding exact location of salt-pepper type noise through eigenvalue analysis of the structure tensor. To resolve two main problems, ramp preserving and removing both normal random noise and salt-pepper type noise, we propose a modified ramp preserving Hahn-Lee method using the eigenvalue analysis scheme.

This paper is organized as follows. The modifications of the ramp preserving Hahn-Lee method are presented in Section 2. The performance evaluation of the proposed method with three different data sets and comparison with other methods are presented in Section 3. The paper is concluded with a summary in Section 4.

## 2 Methodology

### 2.1 Ramp preserving Hahn-Lee Method

The structure tensor  $U$  of data  $I$  is defined by

$$U = \nabla I(x, t) \nabla I(x, t)^T.$$

This matrix has orthonormal eigenvectors  $v_\Lambda$  and  $v_\lambda$  with  $v_\Lambda$  parallel to  $\nabla I$  and the corresponding eigenvalues are given by

$$\Lambda = |\nabla I|^2 \quad \text{and} \quad \lambda = 0.$$

From the geometric point of view,  $U$  is a metric tensor of  $I$ . The eigenvectors  $v_\Lambda$  and  $v_\lambda$  are the directions in which maximum and minimum changes of  $I$  occur, respectively. Also the corresponding eigenvalues  $\Lambda$  and  $\lambda$  denote the amount of changes.

Hahn and Lee [1] proposed a denoising method based on nonlinear partial differential equations (PDEs) with a structure tensor. The proposed model denoises the image  $I$  with the PDEs of the form:

$$\begin{aligned}\frac{\partial I}{\partial t}(x, t) &= \nabla \cdot (g(U)\nabla I(x, t)) & \text{in } \Omega \times (0, T_1], \\ (g(U)\nabla I(x, t)) \cdot \mathbf{n} &= 0 & \text{on } \partial\Omega \times (0, T_1], \\ I(x, 0) &= I_0(x) & \text{on } \Omega,\end{aligned}\tag{2.1}$$

with

$$\begin{aligned}\frac{\partial u_{ij}}{\partial \tau}(x, \tau) &= \nabla \cdot (g(U)\nabla u_{ij}(x, \tau)) & \text{in } \Omega \times (0, T_2], \\ (g(U_\sigma)\nabla u_{ij}(x, \tau)) \cdot \mathbf{n} &= 0 & \text{on } \partial\Omega \times (0, T_2], \\ u_{ij}(x, 0) &= (\nabla I(x, t)\nabla I(x, t)^T)_{ij} & \text{on } \Omega,\end{aligned}\tag{2.2}$$

and

$$g(U) = \frac{1}{\sqrt{1+\Lambda}}v_\Lambda v_\Lambda^T + \frac{1}{\sqrt{1+\lambda}}v_\lambda v_\lambda^T,\tag{2.3}$$

where  $u_{ij} = (U)_{ij}$  and  $\Lambda$  and  $\lambda$  are maximum and minimum eigenvalues of  $U$ , respectively, and  $v_\Lambda$  and  $v_\lambda$  are corresponding eigenvectors.

Note that each time step of numerical implementation of the Hahn-Lee method consists of three parts: construction of the structure tensor  $U$ , regularization of the tensor  $U$  with PDE (2.2), and denoising of the image  $I$  with PDE (2.1). The remarkable point is that this method is robust to the tensor regularization time  $T_2$ . This property is useful since measuring the level of noise is a difficult problem in practice.

In the sense that the diffusivity matrix (2.3) in the Hahn-Lee method uses  $\Lambda = |\nabla I|^2$ , it is a natural extension of the diffusivity coefficient in the Perona-Malik method. The notable point in the Hahn-Lee method is that the same diffusivity matrix is used for image denoising (2.1) and tensor regularization (2.2). In general, the first derivatives of a target image are used in diffusion coefficient or diffusivity matrix to keep edges. For that reason, in tensor regularization, the second derivatives of a target image is commonly used. However, for instance, in a one-dimensional image, the absolute values of the second derivatives have a local minimum at edges, and then the tensor information easily smears out near edges. Hence, in order to preserve edges, it is more suitable to use the first derivative information of a target data in tensor regularization also. See [1] for more details.

In the present paper we will denoise the magnetic flux density  $B_z$  obtained from MREIT experiments and utilize the Laplacian of  $B_z$  in the conductivity reconstruction process. To reconstruct reliable conductivity images, we need to apply adequate denoising method on  $B_z$  before the reconstruction procedure. If we apply edge-preserving type denoising methods such as the Perona-Malik method, however, these methods only preserve the positions where  $|\nabla B_z|$  has its local maxima and lose the information of the ramp's end points. Thus the positions where the Laplacian of  $B_z$  has its local maxima will be located inaccurately. To preserve the endpoints of the ramp, that is, the ramp structure, we adopt the tensor

$$u_{ij}(x, 0) = \left( \sum_{k=1}^2 \nabla w_k(x, t)\nabla w_k(x, t)^T \right)_{ij},$$

where  $(w_1(x, t), w_2(x, t))^T = \nabla I_s$  instead of

$$u_{ij}(x, 0) = (\nabla I_s(x, t)\nabla I_s(x, t)^T)_{ij}.$$

Hahn and Lee [1] modified the original Hahn-Lee method to the following ramp preserving denoising scheme:

$$\begin{aligned}\frac{\partial I}{\partial t}(x, t) &= \nabla \cdot (g(U)\nabla I(x, t)) && \text{in } \Omega \times (0, T_1], \\ (g(U)\nabla I(x, t)) \cdot \mathbf{n} &= 0 && \text{on } \partial\Omega \times (0, T_1], \\ I(x, 0) &= I_0(x) && \text{on } \Omega,\end{aligned}$$

with

$$\begin{aligned}\frac{\partial u_{ij}}{\partial \tau}(x, \tau) &= \nabla \cdot (g(U_s)\nabla u_{ij}(x, \tau)) && \text{in } \Omega \times (0, T_2], \\ (g(U_s)\nabla u_{ij}(x, \tau)) \cdot \mathbf{n} &= 0 && \text{on } \partial\Omega \times (0, T_2], \\ u_{ij}(x, 0) &= \left( \sum_{k=1}^2 \nabla w_k(x, t) \nabla w_k(x, t)^T \right)_{ij} && \text{on } \Omega,\end{aligned}$$

and

$$g(U) = \frac{1}{\sqrt{1+\Lambda}} v_\Lambda v_\Lambda^T + \frac{1}{\sqrt{1+\lambda}} v_\lambda v_\lambda^T.$$

We call this scheme as the ramp preserving Hahn-Lee method, abbreviated as the HL method. The only difference with the original Hahn-Lee method is an initial condition of tensor denoising. The HL method preserves high fluctuated ramp structure well as evaluated in [1].

## 2.2 Modified Hahn-Lee Method

The  $B_z$  data has very low fluctuated ramp structure, and thus the HL method does not work successfully for denoising the  $B_z$  data. To adjust the HL method to MREIT, we propose two modifications of the HL method. The first is to magnify data scale and the second is to scale the diffusivity matrix  $g(U)$ .

The magnitude of  $B_z$  is about  $10^{-9} \sim 10^{-6}$ . Too small magnitude of the data can cause more numerical round-off errors. Also it follows that structure tensor has small magnitude, and then the eigenvalues becomes very small. Hence the diffusivity matrix does not have the anisotropic denoising properties. To overcome this trouble we scale  $B_z$  to the normal image scale such as  $[0, 255]$  and then re-scale it after completing denoising.

The next modification is on the diffusivity matrix  $g(U)$ . We add a scale factor  $h(\lambda)$  in  $g(U)$  as

$$g(U) = \frac{1}{\sqrt{1+h(\lambda)\Lambda}} v_\Lambda v_\Lambda^T + \frac{1}{\sqrt{1+h(\lambda)\lambda}} v_\lambda v_\lambda^T,$$

where  $h(\lambda)$  is defined in two manners depending on the noise state of the  $B_z$  data, which can be anticipated from MR images. When noise is randomly distributed,  $h(\lambda)$  is set to be

$$h(\lambda) = \alpha,$$

where  $\alpha$  is the constant larger than 1 so that it magnifies effects of the diffusivity matrix. As we take larger  $\alpha$ , this method recognizes the strength of ramp structure stronger than the original strength.

If the  $B_z$  data is collected from MRI scanning of humans or *in vivo* animals,  $B_z$  partially has salt-pepper type noise near outer layers of bones and gas-filled organs. If we keep denoising process until this noise disappears, the ramp structure which should be preserved also disappears. Hence it is more efficient to treat this noise separately. The second proposed scale factor allows to conduct isotropic smoothing in salt-pepper type noisy regions and ramp preserving denoising in the other regions based on minimum eigenvalues  $\lambda$  of  $U$ .

The formula of the second scale factor is given by

$$h(\lambda) = \begin{cases} 0 & \text{if } \lambda \geq \hat{\lambda}, \\ \alpha & \text{otherwise,} \end{cases}$$

with

$$\hat{\lambda} = \mu + \beta\sigma,$$

where  $\mu$  and  $\sigma$  are the average and the standard deviation of  $\{\lambda(x)\}_{x \in \Omega}$ , respectively. The constant  $\beta$  in the degrading limit  $\hat{\lambda}$  is an increasing value depending on denoising time as

$$\beta = [\gamma \cdot (\text{Denoising time})],$$

where  $[x]$  refers to a maximum integer not exceeding  $x$  and  $\gamma$  is the constant depending on the level of salt-pepper type noise.

The scale factor describes that we find noisy regions where  $\lambda \geq \hat{\lambda}$  and set  $h(\lambda) = 0$  for these regions. If  $h(\lambda) = 0$ , then denoising occurs in both eigenvector directions with the same amount, so the denoising procedure becomes isotropic smoothing. Hence we can smooth the noisy regions fast and preserve ramp structure with this scale factor. The remaining problem is to figure out the noisy regions with  $\lambda$ . As mentioned above, the eigenvector corresponding to a minimum eigenvalue implies the minimal changing direction at the point, and the minimum eigenvalue implies the amount of change in the corresponding eigenvector direction. The large minimum eigenvalues imply that there are large scale of changes in both eigenvector directions,  $v_\Lambda$  and  $v_\lambda$ . This situation occurs near a corner or noisy regions. Because there is no corner in the  $B_z$  data, it is reasonable to consider the region having the large minimum eigenvalue as a noisy region. The one last thing to consider is how to set the degrading limit which is the criterion of noisy regions. Since the amount of noise decreases over time, the degrading limit is defined with the increasing factor  $\beta$  which is proportional to denoising time. The constant  $\gamma$  is selected around  $3 \sim 5$  depending on the level of salt-pepper type noise.

### 3 Numerical Experiments

In this section, we will illustrate denoising results with three different data sets. To evaluate the proposed method, we will also give denoising results with other denoising methods: the isotropic smoothing, the Perona-Malik (PM) method [7], the harmonic decomposition method [6], and the complex diffusion method [8]. To show the effect of denoising procedure, we will give the results as the reconstructed conductivity image. We use CoReHA(Conductivity Reconstructor using Harmonic Algorithms) [9] for the conductivity reconstruction procedure. Notice that CoReHA gives scaled conductivity.

#### 3.1 Simulated data from the simulated phantom

##### 3.1.1 Generating $B_z$ for the simulated phantom

For a test of the proposed denoising techniques, we generate the magnetic flux density  $B_z$  from the simulated phantom which is a modification of the Shepp-Logan head phantom as in Figure 1(a). We define the conductivities as the values in this figure. First, we compute electric potential, and then obtain the magnetic flux density.

The relation between electric potential and conductivity is given by the following equation:

$$\nabla \cdot (\sigma \nabla u_i) = 0 \quad \text{in } \Omega \quad \text{for } i = 1, 2 \quad (3.1)$$

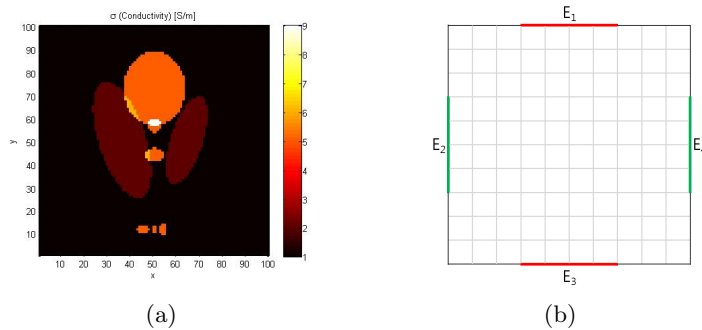


Figure 1: The simulated phantom: (a) conductivity settings, (b) electrode positions.

where  $\sigma$  is the conductivity and  $u_i$ 's are the electric potential. Since two magnetic flux densities are required on the harmonic  $B_z$  algorithm, two different boundary conditions are given:

$$\begin{cases} u_1 = 1 & \text{if } x \in E_2, \\ u_1 = -1 & \text{if } x \in E_4, \\ \nabla u_1 \cdot \mathbf{n} = 0 & \text{otherwise,} \end{cases} \quad (3.2)$$

and

$$\begin{cases} u_2 = 1 & \text{if } x \in E_1, \\ u_2 = -1 & \text{if } x \in E_3, \\ \nabla u_2 \cdot \mathbf{n} = 0 & \text{otherwise,} \end{cases} \quad (3.3)$$

where  $\mathbf{n}$  is a normal vector to  $\partial\Omega$  and  $E_i$ 's are the regions of electrodes as in Figure 1(b). We obtain electric potentials by solving (3.1) twice with these two boundary conditions (3.2) and (3.3). Commonly the  $B_z$  data produced by the horizontal and vertical electric potential difference (i.e., boundary conditions (3.2) and (3.3)) are denoted by  $B_z^1$  and  $B_z^2$ , respectively.

The next procedure is computing  $B_z$  with the Ampere's Law

$$\nabla \times B = \mu_0 J, \quad (3.4)$$

where  $J$  is the electrical current density and  $\mu_0$  is the permeability of free space. A simple calculation leads the following equations:

$$\begin{aligned} -\Delta B_z^i &= \mu_0 \nabla \sigma \cdot (\nabla u_i)^\perp & \text{in } \Omega, \\ \nabla B_z^i \cdot \mathbf{n} &= \mu_0 J_i^\perp \cdot \mathbf{n} & \text{on } \partial\Omega. \end{aligned}$$

The generated  $B_z$  by the above equations is shown in Figures 2(a) and 2(b).

To examine the performance of denoising techniques, we generate Gaussian random noise which has zero mean and the realistic standard deviation. The realistic standard deviation  $\sigma$  with respect to the signal to noise ratio of MR ( $\text{SNR}_{\text{mr}}$ ) is given in [10] as

$$\sigma = \frac{1}{2\gamma T_c \text{SNR}_{\text{mr}}}, \quad (3.5)$$

where the constant  $\gamma$  is the gyromagnetic ratio of hydrogen ( $42.57 \times 10^6 \text{ Hz/T}$ ), the constant  $T_c$  is the effective current application time per excitation ( $24 \times 10^{-3} \text{ A}$ ), and the  $\text{SNR}_{\text{mr}}$  is given by

$$\text{SNR}_{\text{mr}} = \frac{\text{mean of MR on } P}{\text{standard deviation of MR on } P}$$

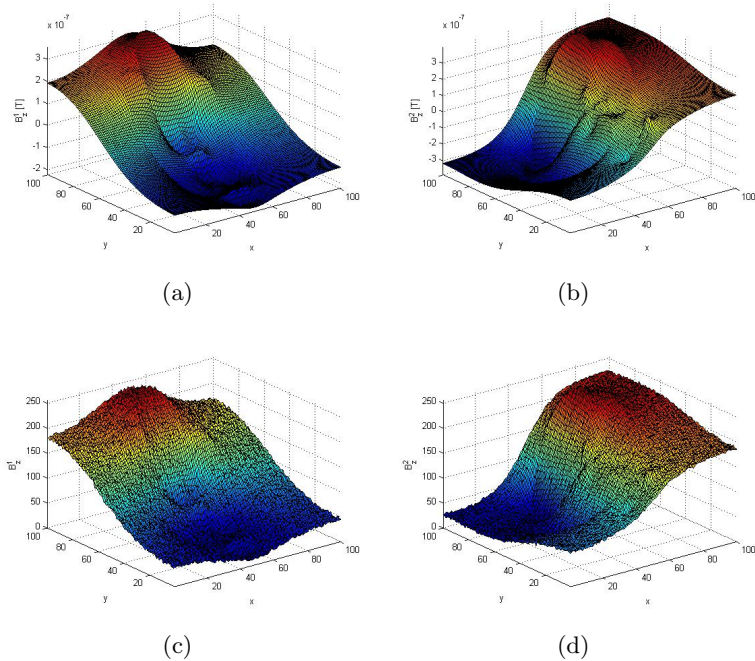


Figure 2: The simulated phantom: (a) simulated clean  $B_z^1$ , (b) simulated clean  $B_z^2$ , (c) simulated noisy  $B_z^1$ , and (d) simulated noisy  $B_z^2$ .

where the region  $P \subset \Omega$  is selected to contain relatively flat MR data to other regions.

Since we are using the simulated data, we do not have MR information. Thus we assume  $\text{SNR}_{\text{MR}}$  value as 90 which is used in [6], and then compute the standard deviation  $\sigma$  from (3.5). After generating Gaussian random noise whose mean is zero and standard deviation is  $\sigma$ , we add the noise to the generated  $B_z$ . Figures 2(c) and 2(d) illustrate the simulated noisy  $B_z$  which are scaled to  $[0, 255]$ . Figures 3(a) and 3(b) illustrate the reconstructed conductivities by the harmonic  $B_z$  algorithm from the simulated  $B_z$  and the simulated noisy  $B_z$ , respectively.

### 3.1.2 Analysis of the Result

We compare the modified HL method with the isotropic smoothing, the PM method, and the complex diffusion method. Since we added Gaussian random noise to  $B_z$ , in the

Denoising method	Denoising time (Coefficient regularization time)	SNR	Rel. $H^1$
Without denoising		0.56	3.137
Isotropic smoothing	1.5	8.97	0.303
PM	2.0 (0.1)	10.78	0.262
Complex diffusion	1.4	10.61	0.264
Modified HL	4.0 (2.0)	11.28	0.244

Table 1: The simulated phantom: Denoising time (Coefficient regularization time) and image quality analysis based on SNR and Rel. $H^1$

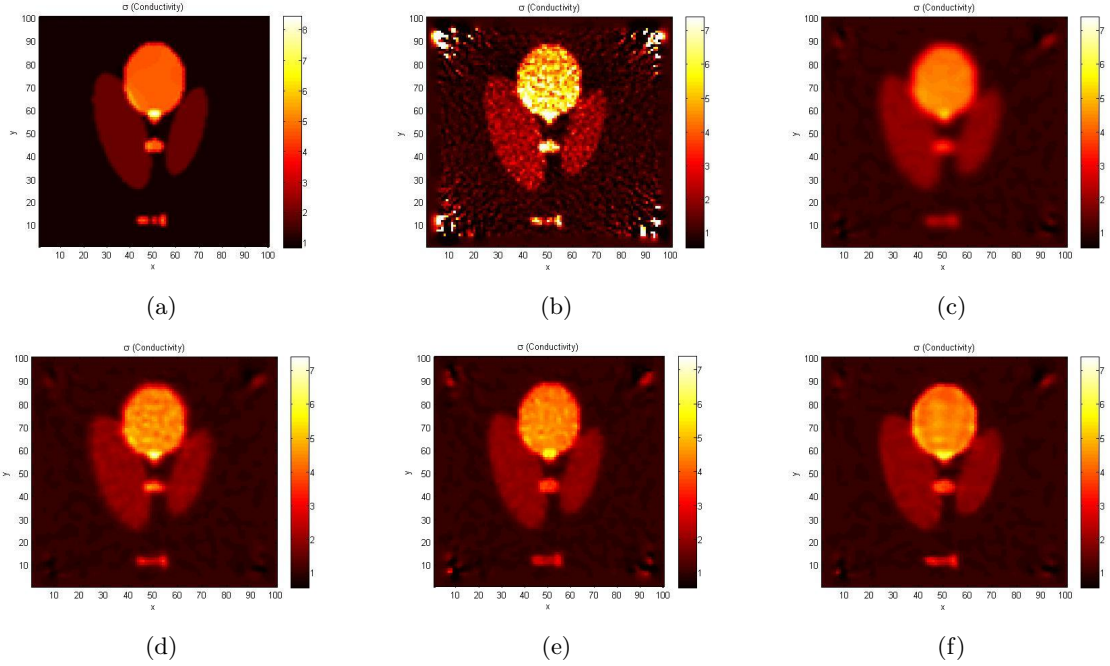


Figure 3: The simulated phantom: reconstructed conductivities in X-Y view. (a) from the simulated clean  $B_z$ , (b) from the simulated noisy  $B_z$  without denoising, (c) from the simulated noisy  $B_z$  with denoising by the isotropic smoothing, (d) the PM method, (e) the complex diffusion method, and (f) the modified HL method.

modified HL method, we utilize the first scale factor

$$h(\lambda) = 10. \quad (3.6)$$

Figure 3(b) shows that there are extreme peaks at the four corners produced while reconstruction procedure. Since the reconstruction algorithm is very sensitive in corners, if the data in corner contains small amount of noise, it results in extreme peaks in reconstructed results. The denoising times of each methods are described in Table 1. In the complex diffusion method and the modified HL method, we terminate denoising processes when the measures defined below have the best values. In the isotropic smoothing and the PM method, when the results have the best quality in the manner of the same measures, they still contain too much noise to distinguish inside features from noise. Thus we also considered whether inside features are distinguishable in determining denoising time for the isotropic smoothing and the PM method.

We evaluate reconstructed results with the signal to noise ratio (SNR) and the relative  $H^1$  norm error (Rel. $H^1$ ). The two measures are given by

$$\text{SNR} = 10 \log_{10} \frac{V(I_r)}{V(I_r - I_o)},$$

$$\text{Rel.}H^1 = \frac{\|I_r - I_o\|_{H^1}}{\|I_o\|_{H^1}},$$

where  $I_r$  is the result,  $I_o$  is the original data,  $V(I)$  is the variance of  $I$ , and  $\|\cdot\|_{H^1}$  is defined as

$$\|I\|_{H^1}^2 = \int_{\Omega} I^2 + \int_{\Omega} |\nabla I|^2.$$

In this analysis,  $I_o$  is the original conductivity settings as in Figure 1(a), and  $I_r$  is a reconstructed conductivity. It is difficult to compare results with denoised  $B_z$  due to the weak ramp structure of  $B_z$ . Also, our goal is reconstructing reliable conductivity images. Thus, we use conductivity images for the comparisons instead of denoised  $B_z$ . If we set  $I_r$  to the reconstructed conductivity in Figure 3(a) obtained from the simulated clean  $B_z$ , SNR is 15.39 and  $\text{Rel.}H^1$  is 0.164. These quantities are the maximal possible SNR and the minimal possible  $\text{Rel.}H^1$ . The SNR and  $\text{Rel.}H^1$  of reconstructed conductivities from denoised  $B_z$  are presented in Table 1. The comparison from Table 1 shows that the results of the modified HL method have the largest SNR and the smallest  $\text{Rel.}H^1$ , so it possesses the closest qualities to the reconstructed conductivity from the simulated clean  $B_z$ .

Figures 3(c), 3(d), 3(e), and 3(f) illustrates images of reconstructed conductivities from denoised  $B_z$ . In the figures, we set data ranges equal in order to compare clearly. If there are values which are not in the fixed data range, they are presented as the same color with the maximum or minimum value in 2-D view or they are chopped off in 3-D view. Compared to the other methods, the results from the modified HL method produces sharp edges, and also it preserves the area of each portions almost exactly. This successful result comes from that we preserve the ramp structure of  $B_z$  effectively by magnifying the strength of ramp structure using the scale factor.

## 3.2 MREIT experimental data from the agar phantom

We now compare the denoising techniques using MREIT experimental data. The experiment was conducted with the agar phantom as shown in Figure 4. The three different objects made of agar are placed in saline solution. The conductivity of upper and lower right objects is fourteen times that of saline water and the conductivity of lower left object is eight times that of saline water.

### 3.2.1 Preprocess for denoising procedure

Let  $\Omega$  be the measuring region and  $S$  be the target denoising region as in Figure 4(b). The main purpose is removal of noise inside  $S$ , however, it leads cumbersome works to set the computing domain to be  $S$ . Thus it is desirable to maintain the computing domain to be  $\Omega$ , but the data on surrounding regions contain a large amount of noise (Figures 5(a) and 5(b)). Because these noises come into  $S$  while denoising, it is required to remove them in advance. Degrading the data of  $S^c$  to 0 may cause numerical problems due to discontinuities, therefore, we extend the data from  $\partial S$  to  $S^c$  harmonically, that is,

Denoising method	Denoising time (Coefficient regularization time)	
	Agar phantom	Post-mortem canine brain
Isotropic smoothing	1.0	0.4
PM	1.0 (0.1)	0.4 (1.0)
Harmonic decomposition	4.75	1.2
Complex diffusion	1.1	3.2
Modified HL	2.7 (2.0)	1.5 (2.0)

Table 2: The agar phantom and the post-mortem canine brain: Denoising time (Coefficient regularization time)

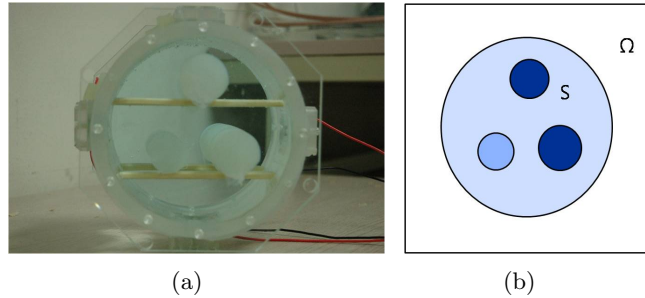


Figure 4: The agar phantom: (a) picture of phantom, (b) illustration.

we solve the following equation

$$\begin{aligned} \Delta B_z &= 0 && \text{in } S^c, \\ \nabla B_z \cdot \mathbf{n} &= 0 && \text{on } \partial\Omega, \\ B_z &= B_z|_{\partial S} && \text{on } \partial S. \end{aligned}$$

The  $B_z$  on the region of  $S^c$  becomes smooth after the extension as in Figures 5(c) and 5(d), while the original  $B_z$  is rugged as in Figures 5(a) and 5(b).

### 3.2.2 Analysis of the Result

Figures 6, 7, and 8 illustrate reconstructed results using denoised  $B_z$  with five denoising methods: the isotropic smoothing, the PM method, the harmonic decomposition method, the complex diffusion method, and the modified HL method. In the modified HL method, we utilize the first scale factor of

$$h(\lambda) = 100,$$

since the noise in the measured  $B_z$  (Figures 5(c) and 5(d)) has the similar feature with randomly distributed noise. Furthermore, since the ramp structure in  $B_z$  data from the agar phantom is weaker than that from the simulated phantom in Section 3.1, we utilize the ten times larger scale factor than (3.6). Table 2 describes denoising times of each methods. We terminate each denoising method when each of the five methods produces its best result and the data distribution in background of reconstructed conductivity are in  $[0.8, 1.2]$ . Since the boundary conductivity is set to be 1 in the harmonic  $B_z$  algorithm, we choose the criterion to be  $[0.8, 1.2]$  for the background error tolerance. Since the harmonic decomposition method needs long denoising time in denoising the background noise, the local features are also smoothed a lot as shown in Figures 6(d) and 7(d).

In Figure 6, we see that the results except from the harmonic decomposition method seem to have similar features. In Figure 7, the amplitudes of results are similar to each other, however, the remarkable contrast is detected from ramp structure. Let us focus on the left-hand side ramp of the middle object of the phantom in magnified views Figure 8. While the result without denoising (Figure 8(a)) possesses sharply breaking curve, there is no breaking region in the ramps of the results from the isotropic smoothing, the PM method and the harmonic decomposition method (Figures 8(b), 8(c), and 8(d)). In contrast to the other results, the ramps of the results from the complex diffusion method and the modified HL method (Figures 8(e) and 8(f)) retain the same structure as in Figure 8(a). Comparing the results between the complex diffusion method and the modified HL method, more detailed features are found in the modified HL method. In this aspect, it is clear that the modified HL method removes noise with preserving ramp structure most successfully.

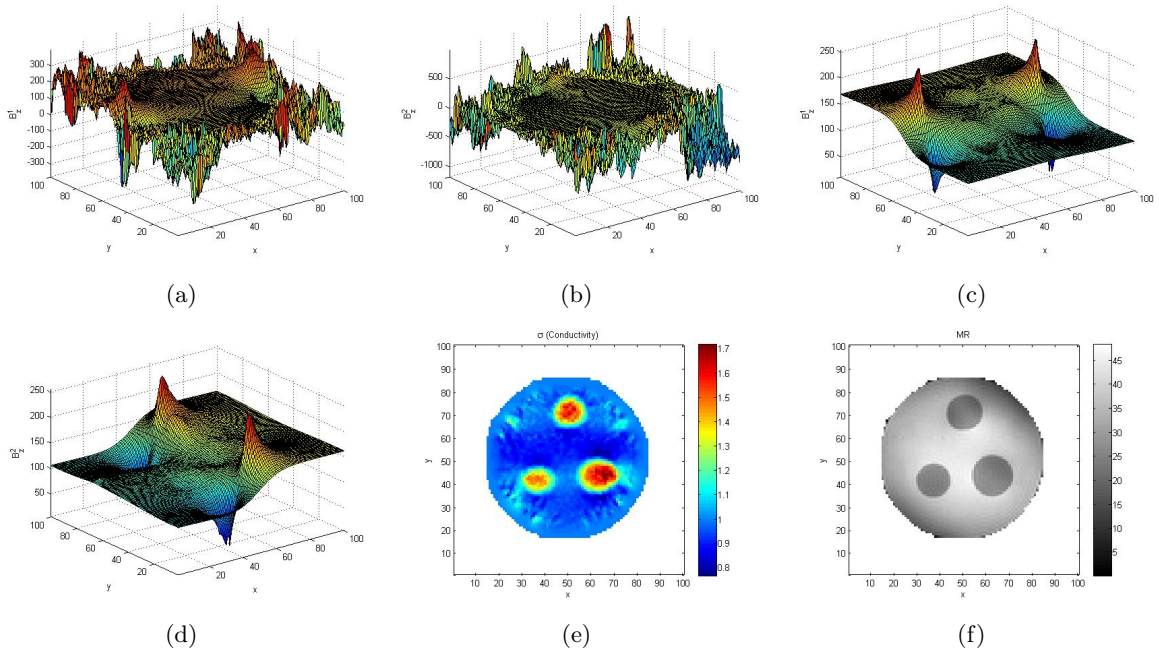


Figure 5: The agar phantom: (a) raw  $B_z^1$ , (b) raw  $B_z^2$ , (c) extended  $B_z^1$ , (d) extended  $B_z^2$ , (e) reconstructed conductivity with raw  $B_z$ , and (f) MR image.

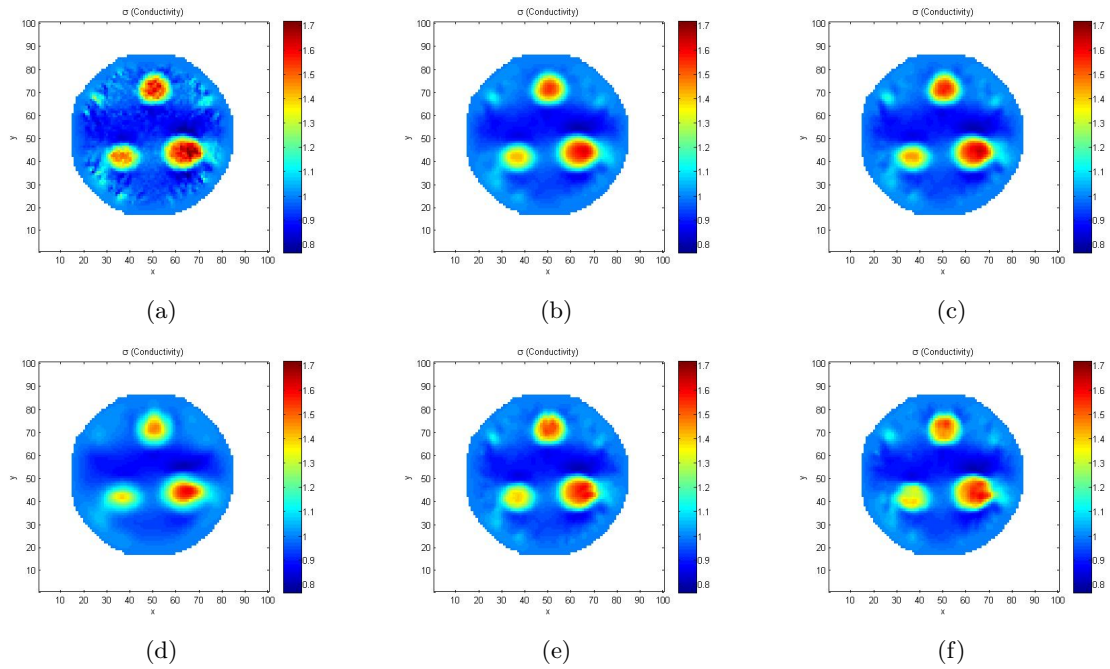


Figure 6: The agar phantom: reconstructed conductivities in X-Y view. (a) without denoising, and with denoising by (b) the isotropic smoothing, (c) the PM method (d) the harmonic decomposition method, (e) the complex diffusion method, and (f) the modified HL method.

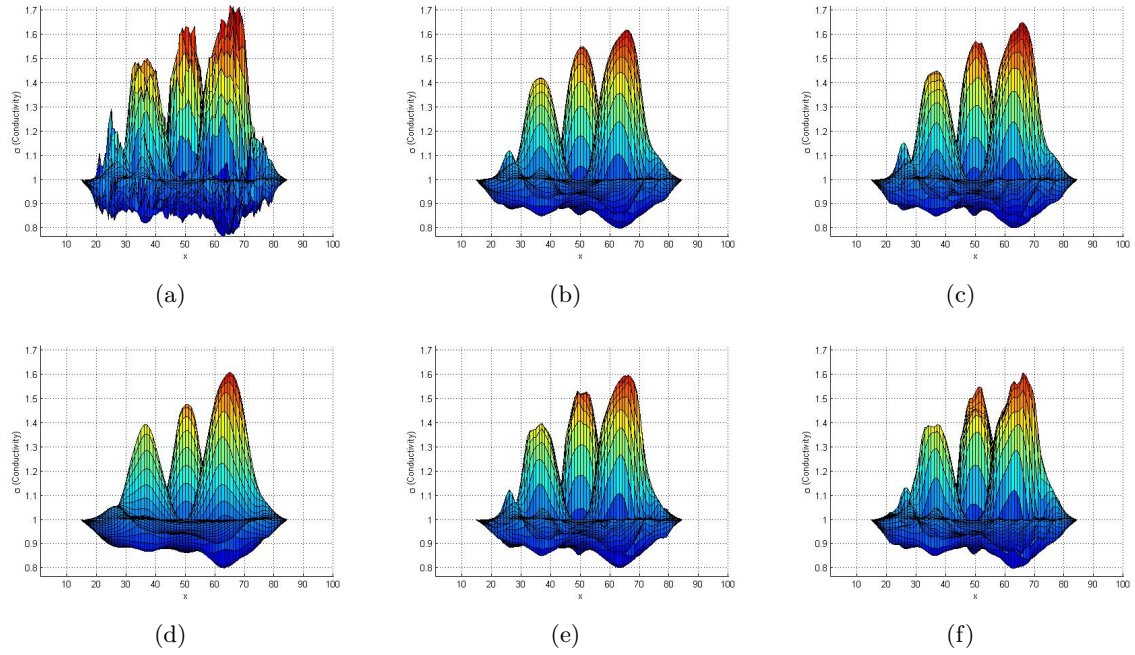


Figure 7: The agar phantom: reconstructed conductivities in X-Z view. (a) without denoising, and with denoising by (b) the isotropic smoothing, (c) the PM method, (d) the harmonic decomposition method, (e) the complex diffusion method, and (f) the modified HL method.

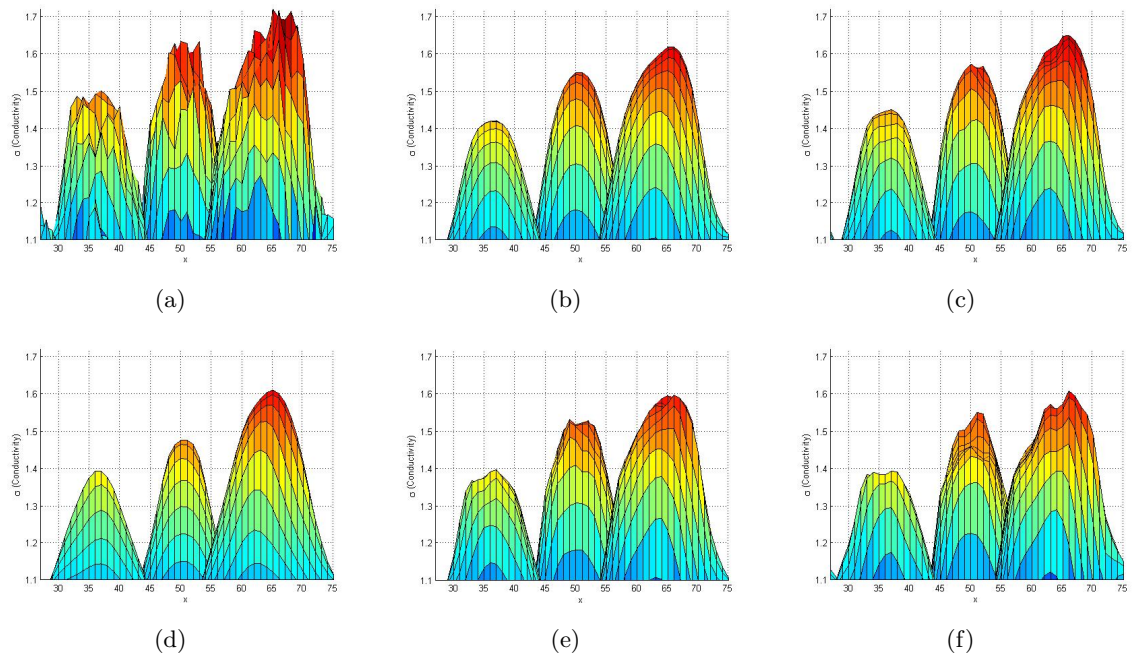


Figure 8: The agar phantom: magnified views of Figure 7. (a) without denoising and with denoising by (b) the isotropic smoothing, (c) the PM method, (d) the harmonic decomposition method, (e) the complex diffusion method, and (f) the modified HL method.

### 3.3 MREIT experimental data from the post-mortem canine brain

In this section, MREIT data from the post-mortem canine brain will be examined. In animal experiments, one of the most problematic issues is salt-pepper type noise produced in outer layers of bones and gas-filled organs. Our  $B_z$  data also contain salt-pepper type noise around a skull of canine head. Looking at the MR image in Figure 9(f), we notice that the upper middle portion is a brain. In this portion, a black region is a skull, M-shape gray region is white matter, and the region between the skull and the white matter is gray matter. Let us focus on  $B_z^1$  and  $B_z^2$  data of the brain part. Figures 10(a) and 10(b) are the magnified views of the brain part of Figures 9(c) and 9(d), respectively. As shown in these figures, a skull causes extreme peaks around the brain part. Furthermore, these peaks in  $B_z$  causes extreme peaks in the reconstructed conductivity. These peaks can be found as discontinuous regions as shown in Figure 9(e). Because the state of noise in this region is different from the other regions, it is reasonable that the denoising procedure is treated separately.

#### 3.3.1 Analysis of the Result

Figures 11 and 12 describe reconstructed results using denoised  $B_z$  with five denoising methods: the isotropic smoothing, the PM method, the harmonic decomposition method, the complex diffusion method, and the modified HL method. In the modified HL method, since the measured  $B_z$  data contain salt-pepper type noise, we utilize the second scale factor of

$$h(\lambda) = \begin{cases} 0 & \text{if } \lambda \geq \hat{\lambda}, \\ 100 & \text{otherwise,} \end{cases}$$

with

$$\begin{aligned} \hat{\lambda} &= \mu + \beta\sigma, \\ \beta &= [3 \cdot (\text{Denoising time})], \end{aligned} \tag{3.7}$$

where  $\mu$  and  $\sigma$  are the average and the standard deviation of  $\{\lambda(x)\}_{x \in S}$ , respectively. Table 2 describes denoising times of each methods. We continue each of denoising procedure until extreme noise peaks disappear.

It is desired that we retain the conductivity information of brain in denoising procedure. For better analysis, we magnify the brain portion of Figure 11 as shown in Figure 12. In contrast to the other results, Figure 12(f) does not contain any noise peaks and it also retains the information of the M-shape white matter distinctly. We also observe the M-shape local features in the other results, however their structure is smooth while the M-shape local features in Figures 12(a) and 12(f) have sharp structures. Furthermore, if we continue denoising using the isotropic smoothing, the PM method, the harmonic decomposition method, and the complex diffusion method until small noise peaks disappear, then the ramp structures of white matter smear out, so we cannot distinguish the white matter from the gray matter.

In the modified HL method, the successful denoising is possible since we are able to identify the noisy regions from the proposed scale factor. The scale factor detects the noisy regions using the minimum eigenvalue distribution of tensor computed from  $B_z$ . If at some point the minimum eigenvalue is larger than the degrading limit in (3.7), we execute isotropic smoothing at the point. Figure 10 presents  $B_z$  information before denoising. There are salt-pepper type noisy regions in  $B_z^1$  and  $B_z^2$ . Comparing 2-D views, we notice that the locations of the noisy regions of Figures 10(c) and 10(d) are identical to the white parts of Figures 10(e) and 10(f). The white parts refer to the regions which have a larger minimum eigenvalue than the degrading limits. Since we compute isotropic smoothing for the white parts, i.e., salt-pepper type noisy regions, we are able to remove the noise fast, while at the same time, preserving ramp structure surrounded by highly oscillated noises.

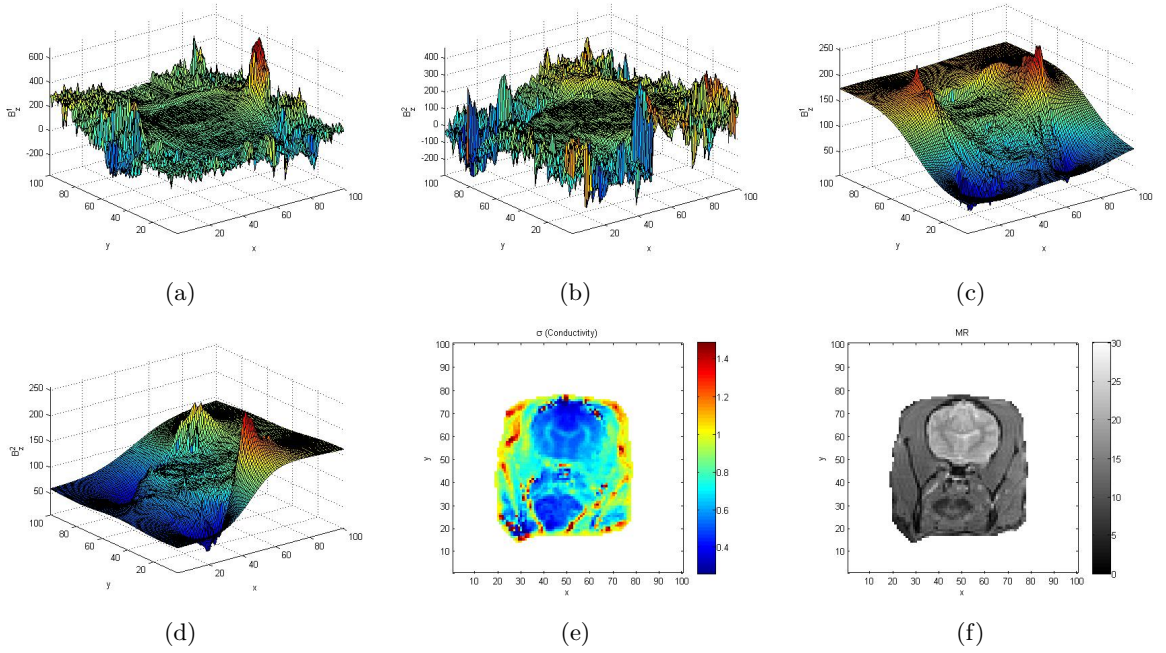


Figure 9: The post-mortem canine brain: (a) raw  $B_z^1$ , (b) raw  $B_z^2$ , (c) extended  $B_z^1$ , (d) extended  $B_z^2$ , (e) reconstructed conductivity with raw  $B_z$ , and (f) MR image.

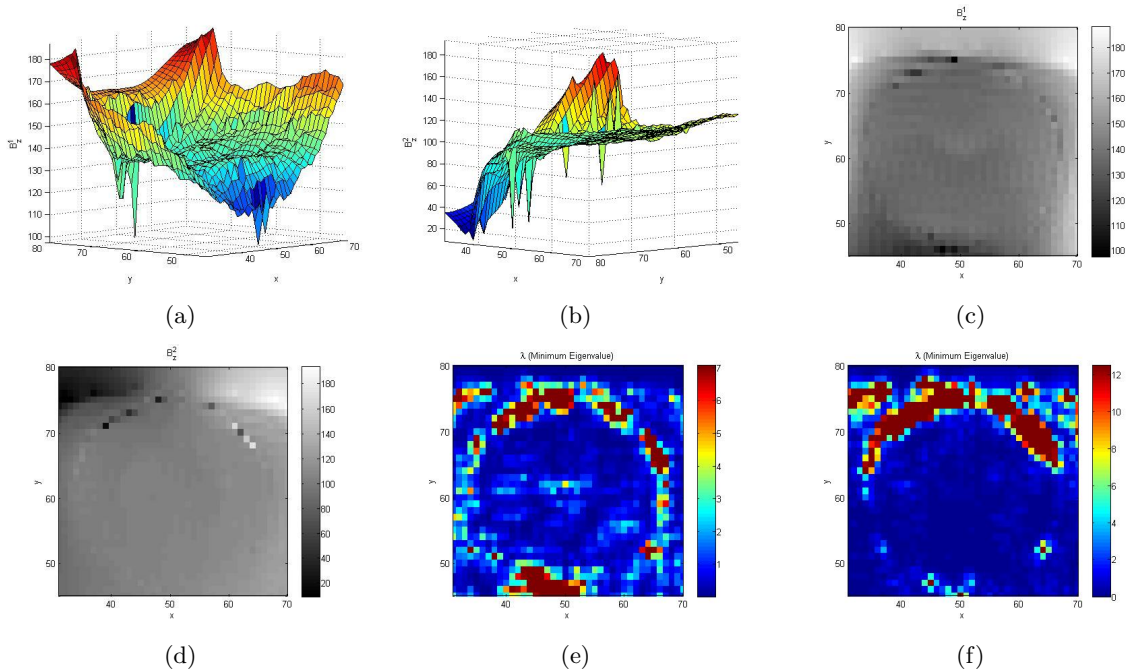


Figure 10: The post-mortem canine brain: magnified views of the brain part before denoising. (a)  $B_z^1$  and (b)  $B_z^2$  in 3-D view, (c)  $B_z^1$  and (d)  $B_z^2$  in 2-D view, (e) minimum eigenvalue distribution of tensor from  $B_z^1$ , and (f) minimum eigenvalue distribution of tensor from  $B_z^2$ .

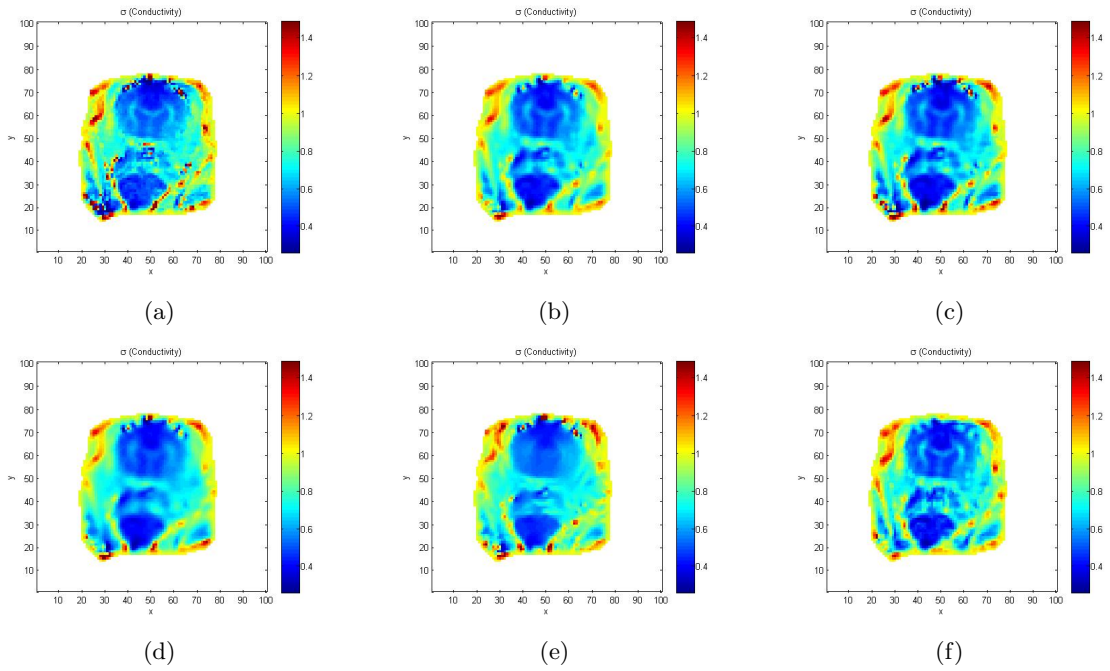


Figure 11: The post-mortem canine brain: reconstructed conductivities in a X-Y view. (a) without denoising, and with denoising by (b) the isotropic smoothing, (c) the PM method, (d) the harmonic decomposition method, (e) the complex diffusion method, and (f) the modified HL method.

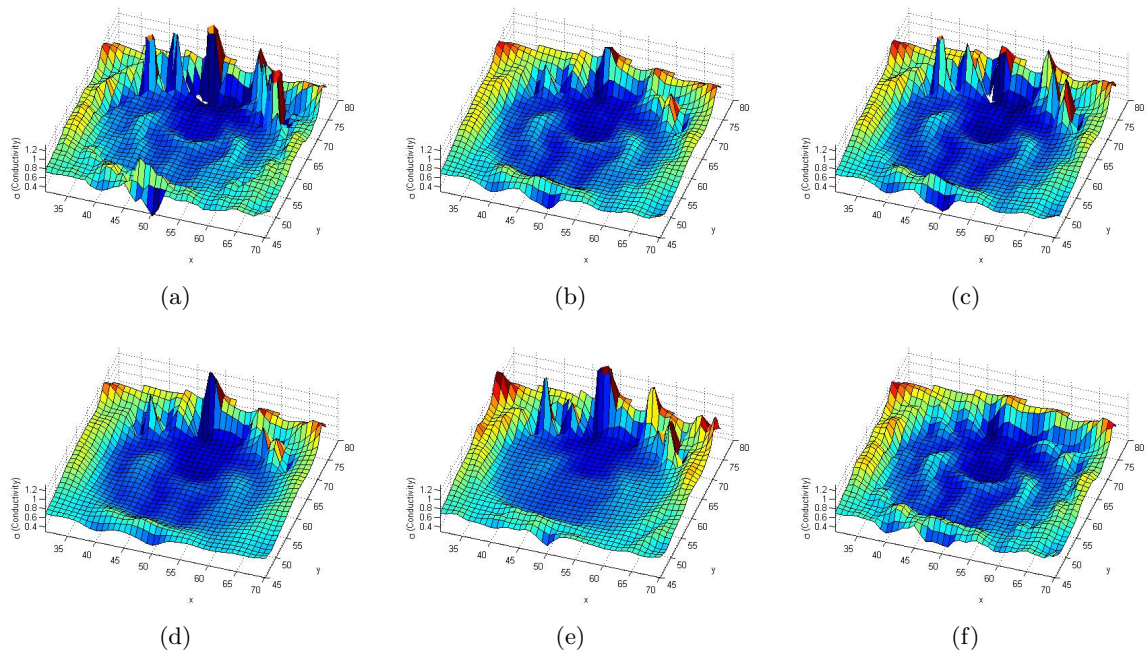


Figure 12: The post-mortem canine brain: 3-D magnified views of the brain part of Figure 11. (a) without denoising, (b) the isotropic smoothing, (c) the PM method, (d) the harmonic decomposition method, (e) the complex diffusion method, and (f) the modified HL method.

## 4 Conclusions

We proposed modifications of the HL method. The HL method is remarkable in its ability to remove noise from normal images, however, for MREIT applications, modifications of the diffusivity matrix are necessary. In MREIT imaging, the HL method performs similarly to isotropic smoothing due to the fact that the data is microscale and the ramp structure is very weak. Thus, we have proposed two noise-feature dependent scale factors of the diffusivity matrix in the nonlinear PDE of the HL method, and confirmed their effectiveness in retrieving information from noisy data: a simulated phantom, an experimental phantom, and a post-mortem canine brain. A main reason for the success of the proposed method is that the scale factor magnifies the effects of ramp-strength and identifies salt-pepper type noisy regions through eigenvalue analysis, thus the method effectively denoises the target by isotropically smoothing salt-pepper type noise while preserving ramp structure.

For broader MREIT applications, it is compulsory that the  $B_z$  data is denoised through preprocessing. In *in vivo* experiments, we cannot use high magnitude currents, and this increases the magnitude of noise in  $B_z$ . Since the Laplacian of  $B_z$  is required in the reconstruction procedure, the results will not be reliable without effective denoising. From the evaluation given in this paper, we are convinced that the modified HL method which identifies noisy regions will perform effectively in *in vivo* experiments.

## References

- [1] J. Hahn and C.-O. Lee. A nonlinear structure tensor with the diffusivity matrix composed of the image gradient. *J. Math. Imag. Vis.*, 34:137-151, 2009.
- [2] S. H. Oh, B. I. Lee, E. J. Woo, S. Y. Lee, M. H. Cho, O. Kwon, and J. K. Seo. Conductivity and current density image reconstruction using harmonic  $B_z$  algorithm in magnetic resonance electrical impedance tomography. *Phys. Med. Biol.*, 48:3101-3116, 2003.
- [3] S. H. Oh, B. I. Lee, T. S. Park, S. Y. Lee, E. J. Woo, M. H. Cho, J. K. Seo, and O. Kwon. Magnetic resonance electrical impedance tomography at 3 tesla field strength. *Magn. Reson. Med.*, 51:1292-1296, 2004.
- [4] H. J. Kim, B. I. Lee, Y. Cho, Y. T. Kim, B. T. Kang, H. M. Park, S. Y. Lee, J. K. Seo, and E. J. Woo. Conductivity imaging of canine brain using a 3 T MREIT system: postmortem experiments. *Physiol. Meas.*, 28:1341-1353, 2007.
- [5] H. J. Kim, T. I. Oh, Y. T. Kim, B. I. Lee, E. J. Woo, J. K. Seo, S. Y. Lee, O. Kwon, C. Park, B. T. Kang and H. M. Park. *In vivo* electrical conductivity imaging of a canine brain using a 3 T MREIT system. *Physiol. Meas.*, 29:1145-1155, 2008.
- [6] B. I. Lee, S.-H. Lee, T.-S. Kim, O. Kim, E. J. Woo, and J. K. Seo. Harmonic decomposition in PDE-based denoising technique for magnetic resonance electrical impedance tomography. *IEEE Trans. Biomed. Eng.*, 52:1912-1920, 2005.
- [7] P. Perona and J. Malik. Scale space and edge detection using anisotropic diffusion. *IEEE Trans. Pattern. Anal. Mach. Intell.*, 12:629-639, 1990.
- [8] G. Gilboa, N. Sochen, and Y. Y. Zeevi. Image enhancement and denoising by complex diffusion processes. *IEEE Trans. Pattern. Anal. Mach. Intell.*, 26:1020-1036, 2004.
- [9] K. Jeon, C.-O. Lee, H. J. Kim, E. J. Woo, and J. K. Seo, CoReHA: conductivity reconstructor using harmonic algorithms for magnetic resonance electrical impedance tomography (MREIT). To appear in *J. of Biomed. Eng. Res.*
- [10] G. C. Scott, M. L. G. Joy, R. L. Armstrong, and R. M. Henkelman. Sensitivity of magnetic-resonance current-density imaging. *J. Magn. Reson.*, 97:235-254, 1992.